

Control of BLDC Motor Drive with Single Hall Sensor Considering Angle Compensation

Research paper

Sen Hong¹, Mingyang Luo², Xueqing Wang^{1,*}

¹College of Electrical Engineering, Sichuan University, Chengdu, China

²Meishan CRRC Fastening System CO., LTD., Meishan, China

Received: 28 June, 2023; Accepted: 01 August, 2023

Abstract: The traditional brushless DC motor uses three position sensors to realise six-step reversing control of the motor. The application of three position sensors increases the cost, whereas the sensorless control method represented by the back electromotive force method has the problem of low control accuracy. Therefore, the present research proposes the method of six-step motor reversing control by using single sensor, corrects the motor running state by using the peak–peak difference of phase current in the control process, and resultantly achieves a good control effect. The experimental results prove the control and correction method.

Keywords: BLDC • six-step commutation • single Hall sensor • angle compensation

1. Introduction

With the development of manufacturing industry, the electric motor, as an electric energy conversion device, has become an indispensable part of industrial production and daily life. The brushless DC motor, which was developed in modern times, refers to a motor without brush and commutator, but with DC motor characteristics. Brushless DC motors are widely used in robotics and automation, aerospace, electric vehicles, manufacturing, and military drive systems (Aghili, 2011; Xu et al., 2023; Chen et al., 2023; Shi et al., 2023; Jin et al., 2023; Zhang et al., 2022).

Brushless motors have the advantages of low cost, simple structure, and good reliability compared with brushed motors (Joon et al., 2019), although brushed DC motors are a tolerable choice in a few applications (Vitols et al., 2010; Kroics and Brazis, 2016; Hõimoja et al., 2010). Brushless DC motors are divided into two categories: one is sine wave driven brushless DC motor, also known as permanent magnet synchronous motor (PMSM), whose Electromotive Force(EMF) waveform is sine wave; the other is square-wave driven brushless DC motor, whose EMF is square wave (Pindoriya et al., 2016).

There are two main control methods of brushless DC motor: the first is to use the position sensor to obtain rotor position signal, so as to realise commutation, but the use of multiple position sensors, as well as the structural requirements of motor installation, are relatively high, which increases the cost of motor. The second method is a sensorless control method for sensorless brushless DC motors, which processes the collected voltage or current signals to obtain the position signal of the rotor. At present, the common control methods include the back EMF method, but zero-crossing of EMF cannot be accurately detected when motor is in zero or low speed since EMF is proportional to speed (Ma et al., 2013).

In order to improve the problems associated with the two abovementioned control methods, a method of using a single position sensor to control the operation of brushless DC motor is proposed in the present research, which reduces the requirements and costs of the motor structure, and modifies the control by using the difference of the

* Email: xwang@scu.edu.cn

peak value of the phase current in the operation process of the motor, thereby enabling an improvement in the control effect.

2. The Basic Structure and Control Principles of Brushless DC Motors

2.1. Basic structure of brushless DC motor

The brushless DC motor controlled by square wave is mainly composed of four parts: power supply, a motor body, rotor position detection device, and a control circuit and inverter. Figure 1 shows the basic structure of a square-wave controlled brushless DC motor.

The rotor position detection device is composed of a position sensor, which feeds back the rotor position information to the control circuits; after the control circuit performs sector discrimination against the rotor position, it generates a drive signal for the inverter, which controls the turning off of the six switch tubes of the inverter, causing the inverter to output voltage to the motor body, and the stator winding generates a magnetic field to control the rotation of the motor rotor.

2.2. Control principle of brushless DC motor

For the brushless DC motor driven by square wave, the control is relatively simple, and the six-step commutation control method is usually used. The name of this technique is derived from the control principle where only two phases are energised at any time to create a rotational vector. The third phase is always disconnected. This forms a six-flux vector, and hence the name six-step control. The physical principle of six-step commutation control is based on the electrification of the electrified conductor to produce magnetic field and magnetic pole heterosexual absorption and same-sex exclusion. Based on these two principles, the two coils in the motor will produce their own magnetic field, through the synthesis of vectors, to obtain the synthetic magnetic field; in turn, the synthetic magnetic field will produce torque to the rotor, and make the rotor rotate. When the synthetic magnetic field is orthogonal to the torque, the torque is the largest. Therefore, in order to keep the rotor rotating, the magnetic field generated by the stator winding needs to constantly change in position, and the rotor will rotate in a direction parallel to the synthetic magnetic field.

Firstly, the space area is divided into six sectors. Three Hall sensors are used to obtain the current position, and after obtaining the sector information of the rotor at this time, the corresponding switch tube is switched on and the corresponding magnetic field is generated. For example, when Hall signal is 101 (i.e. $H_A = 1$, $H_B = 0$, $H_C = 1$; when Hall sensor A detects the rotor, $H_A = 1$ is defined, whereas if no rotor is detected, $H_A = 0$ is defined; H_B and H_C are defined in the same way), switching tubes VT3 and VT4 are switched on, current flows in from B-phase and out from A-phase, and the magnetic field generated is shown in Figure 2 (wherein is indicated the direction of the resultant magnetic field in this case and the position of the rotor at this time). When the rotor is rotated to the next sector, the

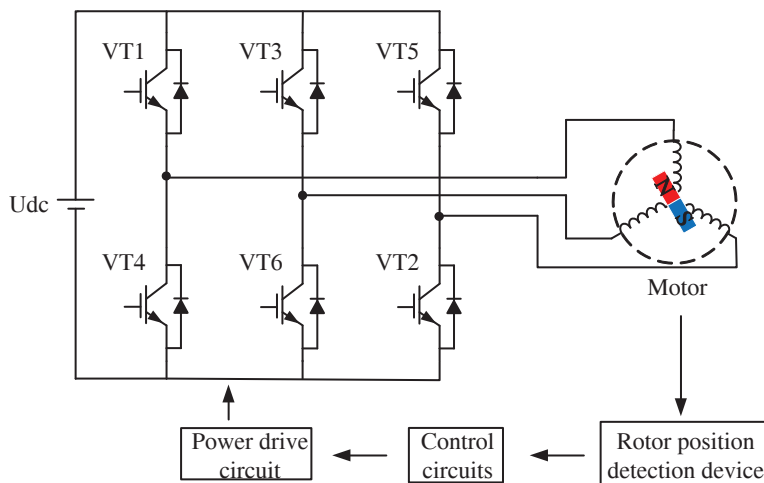


Fig. 1. Basic structure of brushless DC motor.

Hall signal changes to 100, at which point VT4 and VT5 are switched on and current flows in from C-phase and out from A-phase. Thereafter, VT5–VT6, VT6–VT1, VT1–VT2, VT2–VT3, VT3–VT4, and VT4–VT5 are switched on in sequence.

3. Basic Control Principle of Brushless DC Motor with Single Position Sensor

Similar to the case with the control of the three Hall sensors, the core problem faced in achieving single Hall sensor control is the requirement for a means for the detection of the rotor position so as to generate the control signal of the inverter circuit. Single Hall sensor control can be divided into the following steps: (1) position positioning; (2) speed and angle calculation, with sector division; and (3) generation of control signal of inverter circuit.

The positioning method mainly uses the change of Hall sensor value to reflect the two key positions in the rotor rotation process. In this case, the sensor value of the previous interrupt period is defined as H_{A0} . When the sensor value changes from $H_{A0} = 0$ at the previous time to $H_A = 1$ at this time, the electrical angle at this time is defined as $\theta = 0$. When the sensor value changes from $H_{A0} = 1$ at the previous moment to $H_A = 0$ at this moment, the electrical angle at this moment is defined as $\theta = \pi$. Figure 3 shows two key positions for position positioning and their sensor values. A Hall sensor is used to realise two critical positions of the rotor.

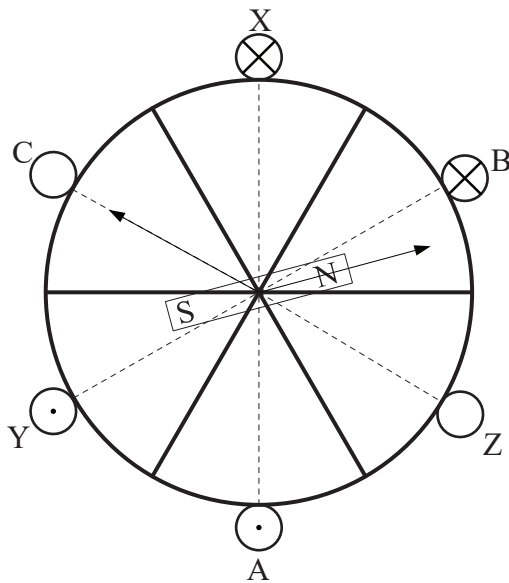


Fig. 2. Synthetic magnetic field.

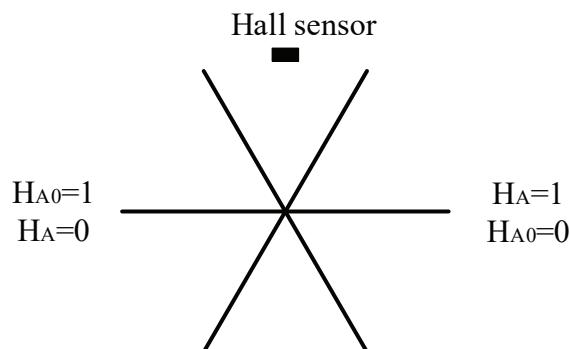


Fig. 3. Location positioning.

The rotor speed can be calculated by using the positioning of Hall sensor. Assuming that the time interval between the last occurrence of $H_{A0} = 0$ and $H_A = 1$ and the next occurrence of $H_{A0} = 1$ and $H_A = 0$ is T (the time interval T can be obtained by entering the interrupt times and the interrupt period), the expression of the angular speed and speed of the rotor can be calculated as follows:

$$w = \frac{\pi}{T} \quad (1)$$

$$n = \frac{30w}{p\pi} \quad (2)$$

where p is the extreme logarithm of the motor. After calculating the speed and angular speed of the motor, the angle can be calculated according to the following formula:

$$\theta = \theta_0 + w\Delta T \quad (3)$$

where ΔT represents the time of an interrupt cycle and θ_0 represents the electrical angle calculated by the previous interrupt cycle. According to the calculated angle, the space of $0-2\pi$ is divided into six sectors, and each sector corresponds to the control signals of different inverter circuits. For example, $0-\pi/3$ corresponds to $H_A = 1$, $H_B = 0$, and $H_C = 1$ (where H_B and H_C represent signals obtained through the θ ; they are equivalent to the signal values of two other sensors when adopting the three Hall sensors control approach). According to this law, the relation among electric angle, the conduction tube, current direction, and H_{ABC} is obtained, as shown in Table 1 (the state H_{ABC} is defined as the calculated value of H_A , H_B , and H_C)

$$H_{ABC} = 4 * H_A + 2 * H_B + H_C. \quad (4)$$

4. Angle Compensation Controlled by a Single Position Sensor of a Brushless DC Motor

When using a Hall sensor for brushless DC motor six-step reversing control, the mechanical installation error of Hall sensor must be considered (Yao et al., 2017; Fang et al., 2014). The actual location of the ideal position, in conjunction with an ahead or lag angle, is considered in the installation of the Hall sensor, as shown in Figure 4, wherein is provided a schematic diagram of the Hall sensor leading and lagging in the ideal position. This error will lead to the advance or lag of the commutation process, resulting in the increase of commutation ripple, operation noise, and steady-state loss and other adverse effects (Xiao et al., 2017; Li et al., 2016).

By detecting the change of phase voltage and DC current before and after commutation, the commutation error of brushless DC motor can be compensated in real time (Chen et al., 2017; Zhou et al., 2017; Fang et al., 2012; Fang et al., 2014; Hõimoja et al., 2010; Lee et al., 2008).

The present researchers have observed that the adverse effects of commutation error on control are intuitively reflected in the peak–peak values of the current. Therefore, to construct a method to correct the angle in the running

H_{ABC}	θ	Conduction tube	Conduction tube
5	0–60	VT3 and VT4	B+A–
4	60–120	VT4 and VT5	C+A–
6	120–180	VT5 and VT6	C+B–
2	180–240	VT6 and VT1	A+B–
3	240–300	VT1 and VT2	A+C–
1	300–360	VT2 and VT3	B+C–

Table 1. Six-step reversing table.

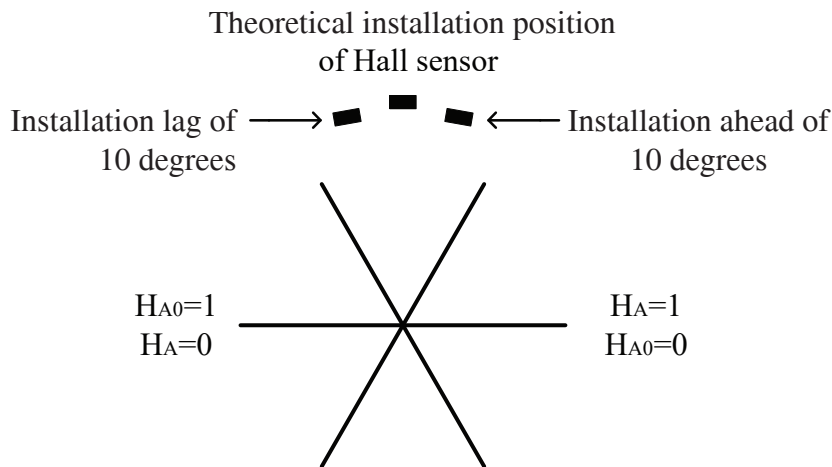


Fig. 4. Hall sensor installation position error diagram.

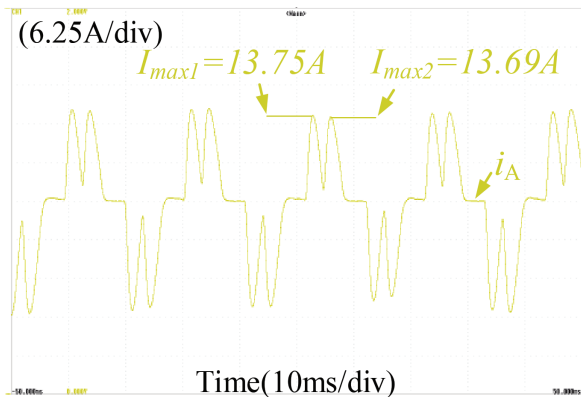


Fig. 5. A-phase current waveform during normal operation.

process, the present research employs the difference between the peak value of phase current in normal operation and the peak value of phase current in leading (lagging) running time.

From the mathematical model of a brushless DC motor, the mathematical expressions for each phase voltage and current can be obtained (Chen et al., 2018). For the current, the amplitude of the current waveform should be the same if the motor parameters and the voltage at both ends of the winding are unchanged, as shown in Figure 5 (taking the A-phase current as an example).

Figures 6 and 7 show the A-phase current waveform of the Hall position sensor installed 10° ahead of the ideal installation position and 10° behind the installation position. As can be seen from the Figures 6 and 7, when there is a deviation in the installation position of Hall sensor, there is a difference in the peak-to-peak value of current. Assuming VT1 is conducting, we define the first current wave peak as I_{max1} and the second current wave peak as I_{max2} , and also define the difference between the two as ΔI .

Figure 6 shows the current waveform when the Hall sensor installation position is 10° ahead of the ideal position. We can notice that I_{max1} is less than I_{max2} . Figure 7 shows the current waveform when the Hall sensor installation position lags behind the ideal position by 10° . We can notice that I_{max2} is less than I_{max1} .

The reason for the difference between the two peaks is that the position installation error of the Hall sensor leads to the lead and lag of the commutation, so that the current in the inductor enters the next on-state without decaying to 0 A. Taking the advance installation of the position sensor as an example, Figure 8 is the waveform diagram of the EMF (A-phase) and the A-phase current and angle when the Hall sensor installation position has no error, and

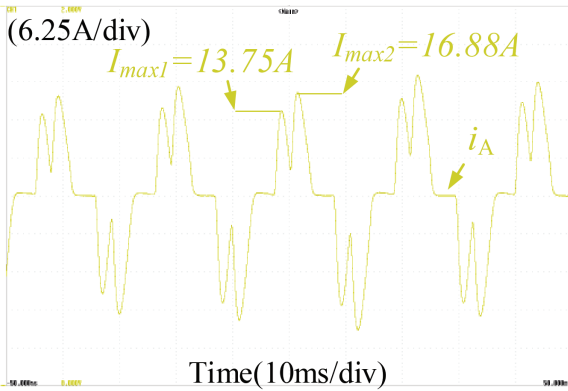


Fig. 6. A-phase current waveform at an angle ahead of 10° .

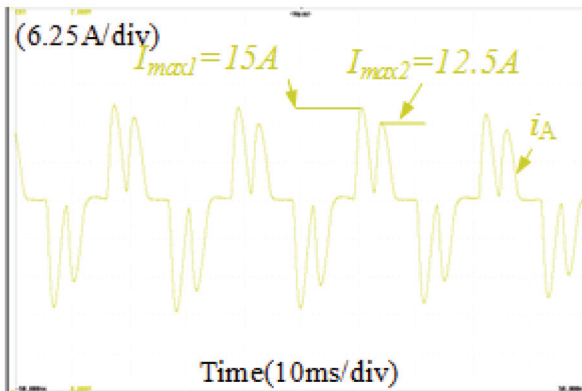


Fig. 7. A-phase current waveform at an angle lag of 10° .

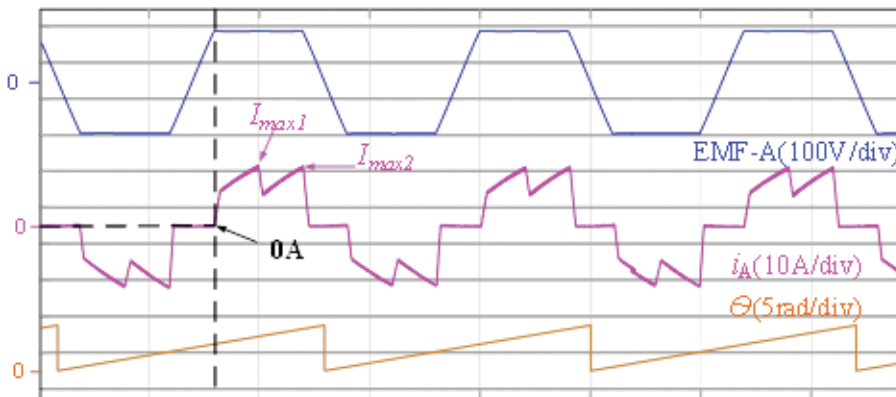


Fig. 8. Waveform of A-phase current, EMF (A-phase), and θ without installation error.

Figure 9 is the waveform diagram of the EMF (A-phase) and the A-phase current and angle when the Hall sensor installation position is 10° ahead of the ideal installation position. It can be seen from Figure 8 that when the Hall sensor installation has no error, when A-phase is positive, the current of A-phase decreases to 0 A (as shown by the black dashed line in Figure 8). As can be seen from Figure 9, when the Hall sensor is installed 10° ahead of time, when the A-phase positive pilot is on, the current of A-phase does not decay to 0 A, and the current is -5 A (as shown by the black dashed line in Figure 9). Therefore, in the case of this installation error, it is necessary to overcome the reverse current formed by the energy stored by the inductor in the previous cycle when the A-phase

positive guide is passed, and so there will be $I_{max1} < I_{max2}$. The analysis of the Hall sensor installation lag of 10° is the same as the above process.

In Code Composer Studio(CCS), we use bubble sort to compute I_{max1} and I_{max2} , and then we can calculate the peak difference ΔI . If ΔI is greater than 0 A, then the delay compensation is entered. Alternatively, if ΔI is less than 0 A, then the lead compensation can be entered. We may take the lead compensation as an example. After the program enters the lead compensation, 0.01 radian is corrected in each interrupt cycle. When the conditions are not met, the compensation ends.

5. Experimental Verification

Figure 10 shows the brushless DC motor experimental platform used in this experiment. On this experimental platform, the control method of single Hall sensor and the correct method of current peak difference are verified.

The experimental platform uses a seven-pole motor. During the experiment, the motor speed was 400 rpm/min. Figure 11 shows the A-phase current waveform and Hall A value. It can be seen from the figure that the waveform of A-phase current is symmetrical, and the corresponding relationship between waveforms of Hall sensor A and A-phase current is consistent with the commutation sequence in Table 1. As shown in the figure, when the value of Hall sensor value is 1, the corresponding current turn-on sequence is B+A-, C+A-, and C+B-, which is consistent with the result of A-phase current waveform.

Figure 12 shows the calculated values of θ , H_{ABC} , and H_A . It shows that the waveform of the θ is a straight line. Meanwhile, it is noted that the value of the electrical angle defined in the position positioning mentioned above does

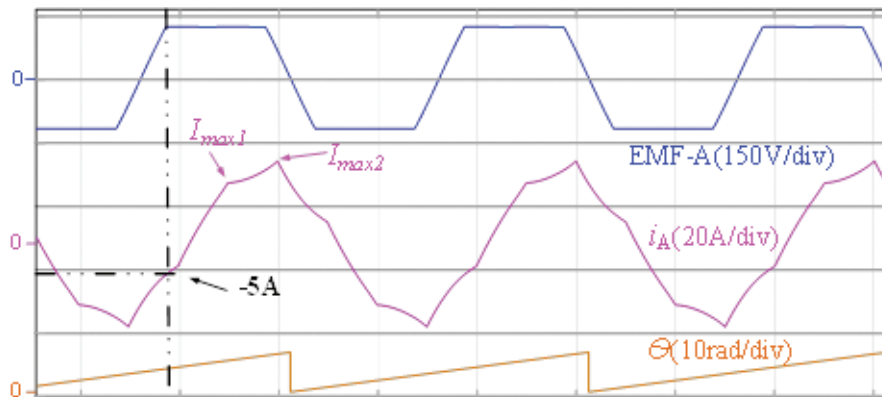


Fig. 9. Waveform of A-phase current, EMF (A-phase), and θ with installation error (10° ahead).

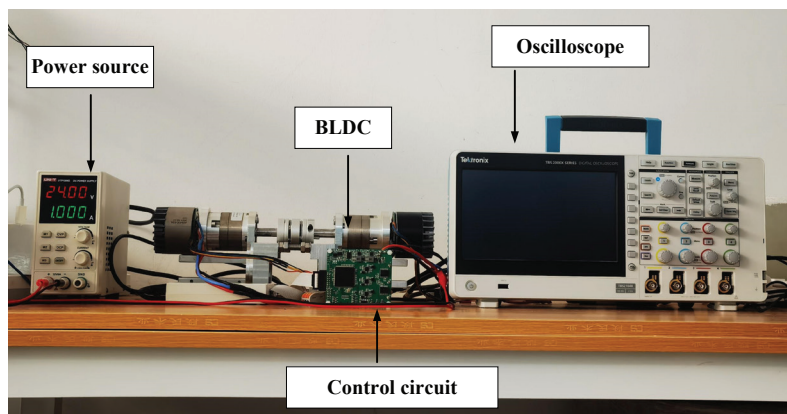


Fig. 10. Experimental platform.

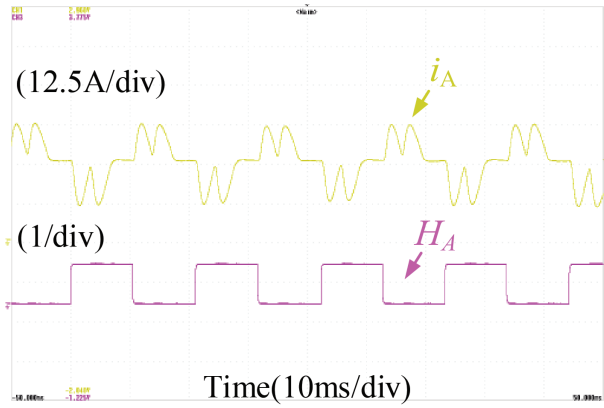


Fig. 11. A-phase current and H_A 's value waveforms.

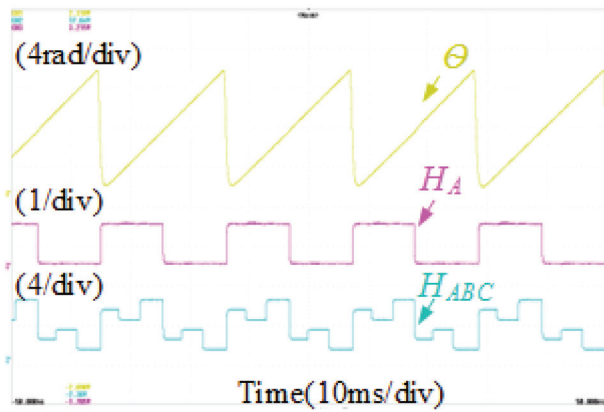


Fig. 12. θ , Hall waveforms.

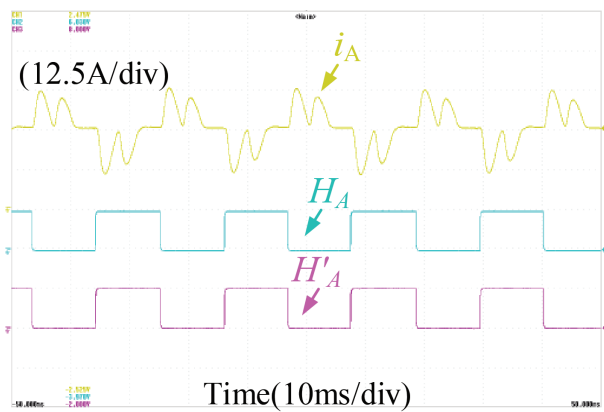


Fig. 13. A-phase current waveform, sensor signal H_A before compensation, and sensor signal H'_A after compensation waveform; no compensation is added at this time.

not cause a sudden change in the angle waveform, indicating that the calculation method of speed and angle is correct. Using the obtained θ , we can obtain the waveform of H_{ABC} .

Figure 13 shows the waveforms of the sensor signal H_A before compensation and the sensor signal H'_A after compensation, with an angle lag of 10° . Due to the absence of compensation at this time, the waveform of the two

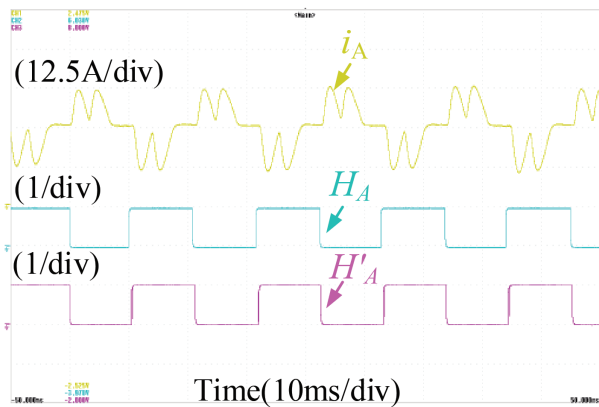


Fig. 14. A-phase current waveform, sensor signal H_A before compensation, and sensor signal H'_A after compensation waveform, with subsequent addition of compensation.

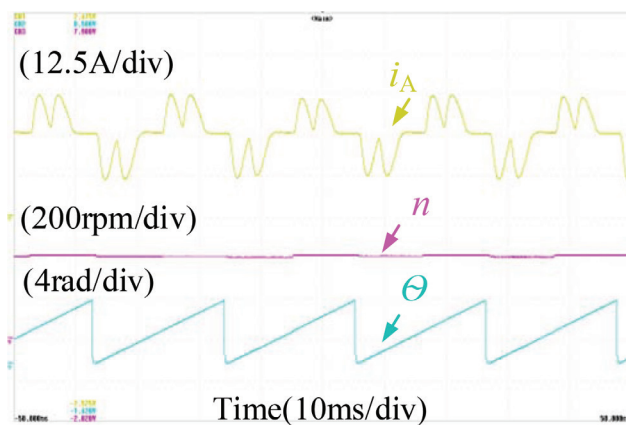


Fig. 15. Waveforms of A-phase current, rotational speed, and θ during stable operation.

signal values should be consistent. It can also be seen from the peak-to-peak value of the current waveform that the position of Hall sensor in the motor used in this experiment is lagging behind the ideal installation position.

In the present research, the fact of whether the absolute value of current amplitude difference before and after compensation is reduced or not is used to reflect whether the compensation is effective. The current waveform in Figure 14 is the current waveform after adding angle compensation. As can be seen from the figure, after adding compensation, the difference between the two peaks decreases significantly. H_A is the signal waveform of Hall sensor without adding compensation, and H'_A is the modified waveform of Hall sensor signal after adding compensation. According to the previous analysis, delay compensation should be added here. Subsequent to adding compensation, the signal waveforms of H_A and H'_A are seen to be characterised by the appearance of phase difference, which represents the compensation angle.

Figure 15 shows the waveforms of current, speed, and electrical angle when the motor is running. The current waveform is consistent with the angle waveform. As can be seen from the figure, by using two critical positioning of the rotor and calculating the times associated with these two positioning, the speed can be updated once every half cycle, and thus the speed will not be the same in the adjacent half cycles. The operating condition set in this experiment is 400 rpm/min. From the speed waveform, the experimental speed can be maintained at about 400 rpm/min, indicating that the control effect and angle correction effect of the single sensor are good.

Through the above analysis of the waveform of the experimental results, it can be seen that the control method and the correction method have a good effect. In order to obtain the advantages of this control method, the proposed control method of unit sensor with angle compensation is compared with the control method of six-step commutation with three-position sensor, and the following advantages are obtained. The first advantage is that the reduction of the number of position sensors used in the control method proposed in the present research will reduce the number

of interfaces of the motor, and the installation requirements of the hardware circuit in the motor will be reduced. The second advantage is that the control method in the present research considers the influence of the installation error of Hall sensor on the operation of the motor, and corrects the error during the control process to improve the accuracy of the control. The six-step commutation control method of the three-position sensor does not consider the installation error of the position sensor.

The main purpose of the present research is to verify the proposed control method and correction method. The above experimental results can prove the correctness of the control method and correction method. Therefore, the dynamic performance of this control method is not evaluated in the present research.

References

- Aghili, F. (2011). Fault-tolerant control of robot servomotors. In: *IEEE International Conference on Robotics and Automation*, Shanghai, China, 09-13 May, 2011, pp. 2757–2763.
- Chen, S., Liu, G. and Zheng, S. (2017). Sensorless Control of BLDCM Drive for a High-Speed Maglev Blower using Low-Pass Filter. *IEEE Transactions on Power Electronics*, 32(11), pp. 8845–8856.
- Chen, S., Sun, W., Wang, K., Liu, K. and Zhu, L. (2018). Sensorless High-Precision Position Correction Strategy for a 100 kW@20 000 r/min BLDC Motor with Low Stator Inductance. *IEEE Transactions on Industrial Informatics*, 14(10), pp. 4288–4299.
- Chen, Y., Wang, X., Meng, X., He, M., Xiao, D. and Wang, Z. (2023). A Universal Model Predictive Control Strategy for Dual Inverters Fed OW-PMSM Drives. *IEEE Transactions on Power Electronics*, 38(6), pp. 7575–7585.
- Fang, J., Li, W. and Li, H. (2014). Self-Compensation of the Commutation Angle Based on DC-Link Current for High-Speed Brushless DC Motors with Low Inductance. *IEEE Transactions on Power Electronics*, 29(1), pp. 428–439.
- Fang, J., Zhou, X. and Liu, G. (2012). Instantaneous Torque Control of Small Inductance Brushless DC Motor. *IEEE Transactions on Power Electronics*, 27(12), pp. 4952–4964.
- Höimoja, H., Vinnikov, D., Lehtla, M., Rosin, A. and Zakis, J. (2010). Survey of loss minimization methods in tram systems. In: *International Symposium on Power Electronics, Electrical Drives, Automation and Motion, SPEEDAM 2010*, Pisa, Italy, 14-16 June, 2010, pp. 1356–1361.
- Jin, L., Mao, Y., Wang, X., Shi, P., Lu, L. and Wang, Z. (2023). Optimization-Based Maximum-Torque Fault-Tolerant Control of Dual Three-Phase PMSM Drives under Open-Phase Fault. *IEEE Transactions on Power Electronics*, 38(2), pp. 3653–3663.
- Joon, S. P., Ki-Doek, L., Sung, G. L. and Won-Ho, K. (2019). Unbalanced ZCP Compensation Method for Position Sensorless BLDC Motor. *IEEE Transactions on Power Electronics*, 34(04), pp. 3020–3024.
- Kroics, K. and Brazis, V. (2016). ‘Supercapacitor based storage system for efficiency improvement of lead-acid powered light electric vehicle. In: *IEEE International Power Electronics and Motion Control Conference (PEMC)*, Varna, Bulgaria, 25-28 September, 2016, pp. 1216–1221.
- Lee, D.-M. and Lee, W.-C. (2008). Analysis of Relationship between Abnormal Current and Position Detection Error in Sensorless Controller for Interior Permanent-Magnet Brushless DC Motors. *IEEE Transactions on Magnetics*, 44(8), pp. 2074–2081.
- Li, W., Fang, J., Li, H. and Tang, J. (2016). Position Sensorless Control without Phase Shifter for High-Speed BLDC Motors with Low Inductance and Nonideal Back EMF. *IEEE Transactions on Power Electronics*, 31(2), pp. 1354–1366.
- Ma, X., Wang, X., Deng, Z., Zhou, P. and Zhao, Y. (2013). Position sensorless starting method of BLDC motor based on SVPWM and stator magnetomotive force control. In: *IECON 2013 – 39th Annual Conference of the IEEE Industrial Electronics Society*, Vienna, 10-13 November, 2013, pp. 3054–3059.
- Pindoriya, R. M., Mishra, A. K., Rajpurohit, B. S. and Kumar, R. (2016). Analysis of position and speed control of sensorless BLDC motor using zero crossing back-EMF technique. In: *IEEE 1st International Conference on Power Electronics, Intelligent Control and Energy Systems (ICPEICES)*, Delhi, India, 04-06 July, 2016, pp. 1–6.
- Shi, P., Wang, X., Meng, X., He, M., Mao, Y. and Wang, Z. (2023). Adaptive Fault-Tolerant Control for Open-Circuit Faults in Dual Three-Phase PMSM Drives. *IEEE Transactions on Power Electronics*, 38(3), pp. 3676–3688.
- Štulrajter, M., Makyšsn, P. and Rafajdus, P. (2017). Sensorless control of high speed BLDC. In: *2017 IEEE International Symposium on Sensorless*

- Control for Electrical Drives (SLED)*, Catania, Italy, 18-19 September, 2017, pp. 225–230.
- Vitols, K., Reinberg, N., Sokolovs, A. and Galkin, I. (2010). Drive selection for electric kart. In: *Proceedings of 14th International Power Electronics and Motion Control Conference EPE-PEMC2010*, Ohrid, Macedonia, 06-08 September, 2010, pp. T9-15–T9-18.
- Xiao, G., Tu, W., Suo, C., Tang, L. and Yang, K. (2017). Research and design of speed control for high speed sensorless brushless DC motor with commutation compensation. In: *2017 20th International Conference on Electrical Machines and Systems (ICEMS)*, Sydney, NSW, Australia, 11-14 August, 2017, pp. 1–5.
- Xu, T., Wang, X., Xiao, D., Meng, X., Mao, Y. and Wang, Z. (2023). A Novel Two-Mode Inverter-Based Open-Winding PMSM Drive and its Modulation Strategies. *IEEE Transactions on Power Electronics*, 38(7), pp. 8762–8774.
- Yao, X., Jiang, X. and Zhang, Y. (2017). Compensation method for commutation torque ripple reduction of BLDC motor with misaligned hall sensors. In: *IECON 2017 – 43rd Annual Conference of the IEEE Industrial Electronics Society*, Beijing, China, 29 October - 01 November, 2017, pp. 1862–1867.
- Zhang, Y., Mao, Y., Wang, X., Wang, Z., Xiao, D. and Fang, G. (2022). Current Prediction-Based Fast Diagnosis of Electrical Faults in PMSM Drives. *IEEE Transactions on Transportation Electrification*, 8(4), pp. 4622–4632.
- Zhou, X., Chen, X., Lu, M. and Zeng, F. (2017). Rapid Self-Compensation Method of Commutation Phase Error for Low- Inductance BLDC Motor. *IEEE Transactions on Industrial Informatics*, 13(4), pp. 1833–1842.